Rapid Prototyping Polymers for Microfluidic Devices and High Pressure Injections

ARTICLE *in* LAB ON A CHIP · NOVEMBER 2011

Impact Factor: 5.75 · DOI: 10.1039/c1lc20514e · Source: PubMed

4 AUTHORS:

Elodie Sollier
Vortex Biosciences, Inc.
23 PUBLICATIONS **373** CITATIONS
SEE PROFILE

Coleman Tyler Murray
University of California, Los Angeles
11 PUBLICATIONS **131** CITATIONS
SEE PROFILE

Pietro Maoddi
CERN
3 PUBLICATIONS **81** CITATIONS
SEE PROFILE

Dino Di Carlo
University of California, Los Angeles
139 PUBLICATIONS **3,646** CITATIONS
SEE PROFILE

Lab on a Chip

Cite this: *Lab Chip*, 2011, **11**, 3752

www.rsc.org/loc

TUTORIAL REVIEW

Rapid prototyping polymers for microfluidic devices and high pressure injections†

Elodie Sollier,* Coleman Murray, Pietro Maoddi and Dino Di Carlo*

Received 13th June 2011, Accepted 9th September 2011
DOI: 10.1039/c1lc20514e

Multiple methods of fabrication exist for microfluidic devices, with different advantages depending on the end goal of industrial mass production or rapid prototyping for the research laboratory. Polydimethylsiloxane (PDMS) has been the mainstay for rapid prototyping in the academic microfluidics community, because of its low cost, robustness and straightforward fabrication, which are particularly advantageous in the exploratory stages of research. However, despite its many advantages and its broad use in academic laboratories, its low elastic modulus becomes a significant issue for high pressure operation as it leads to a large alteration of channel geometry. Among other consequences, such deformation makes it difficult to accurately predict the flow rates in complex microfluidic networks, change flow speed quickly for applications in stop-flow lithography, or to have predictable inertial focusing positions for cytometry applications where an accurate alignment of the optical system is critical. Recently, other polymers have been identified as complementary to PDMS, with similar fabrication procedures being characteristic of rapid prototyping but with higher rigidity and better resistance to solvents; Thermoset Polyester (TPE), Polyurethane Methacrylate (PUMA) and Norland Adhesive 81 (NOA81). In this review, we assess these different polymer alternatives to PDMS for rapid prototyping, especially in view of high pressure injections with the specific example of inertial flow conditions. These materials are compared to PDMS, for which magnitudes of deformation and dynamic characteristics are also characterized. We provide a complete and systematic analysis of these materials with side-by-side experiments conducted in our lab that also evaluate other properties, such as biocompatibility, solvent compatibility, and ease of fabrication. We emphasize that these polymer alternatives, TPE, PUMA and NOA, have some considerable strengths for rapid prototyping when bond strength, predictable operation at high pressure, or transitioning to commercialization are considered important for the application.

1. Introduction

Various methods of fabrication exist for microfluidic devices,[1–3] depending on the end goal of industrial mass production or rapid prototyping at the research laboratory level. Each application area has different constraints such that there is still a gap between academic and industrial practices.[4] Rapid prototyping methods suitable for research laboratories possess characteristics including (i) a short fabrication time and (ii) a low-cost for a complete cycle, from the design of the geometry, to its fabrication, packaging and testing (Fig. 1). Indeed, the rapid prototyping of microfluidic systems is used in the exploratory stages of the development of microdevices, when new ideas have to be quickly tested. Rapid prototyping should also ideally facilitate the transfer of efficient designs from the research laboratory level to high-volume production without significant redesigns – requiring materials with similar physical and chemical properties.

Glass and silicon micro-machining

Highly developed to fabricate microelectromechanical systems, glass and silicon micro-machining is commonly used for microfluidic devices due to its fidelity in achieving small feature resolution, surface stability and solvent compatibility.[5–7] Especially, glass is a material of choice in microfluidics due to its beneficial optical properties, and the strength of anodic bonding which allows an excellent resistance to high pressures.[8] However, use for rapid prototyping is strongly limited due to the need for clean room equipment and facilities and the high cost involved in processing and the material itself. Additionally, glass micromachining processes are technically demanding and time consuming.

Department of Bioengineering, Henry Samueli School of Engineering and Applied Science, University of California, Los Angeles, CA, 90095. E-mail: elodie.sollier@yahoo.fr; dicarlo@seas.ucla.edu.
† Electronic supplementary information (ESI) available. See DOI: 10.1039/c1lc20514e

Polymer molding and machining

Polymers, such as Polystyrene (PS),[9,10] Polycarbonate (PC),[11–13] Polyvinyl chloride (PVC),[13] Cyclic Olefin Copolymer (COC)[10,14] and especially Poly(methyl methacrylate) (PMMA),[10–17] offer an attractive alternative to glass and silicon for rapid prototyping, as they are cheaper, robust, and generally have faster fabrication processes. Fabrication is usually based on three families of techniques: injection molding/hot embossing, polymer micro-machining/laser ablation, and polymer casting.[3,18]

(i) Polymer thermoforming. *Injection molding*, commonly used for many plastic products, involves the high pressure injection of melted thermoplastic pellets into a heated mold. Even though experimental parameters must be optimized for each production run, injection molding offers a high-throughput fabrication option. However, because of the complexity and high initial cost of the molding equipment and masters, injection molding is rarely used for rapid prototyping.[19,20] Alternatively, *hot embossing* is a fabrication method which consists of pressing a heated silicon or metal mold against a thermoplastic sheet, such as PMMA or COC[4] to form device features. Embossing is fast and less expensive than injection molding, but still requires dedicated press equipment, a robust mold, and suffers from a lack of convenient methods for strong bonding.[11] However, recent studies demonstrated an enhanced thermoforming method for microstructures with simplified equipment,[21] or

Elodie Sollier

Elodie Sollier is a Postdoctoral Researcher in the Microfluidic Biotechnology Laboratory, at the University of California, Los Angeles under Professor Dino Di Carlo. After a Physical Engineering Degree from Institut National Polytechnique de Grenoble in 2006, she received her Ph.D in Physics for Life Science in 2009, from the University of Grenoble and CEA LETI Minatec. Her Ph.D work was focused on the development of passive and continuous microfluidic approaches for blood sample preparation. Her current research interests include developing new biological applications for inertial microfluidics, and microfabrication approaches for transitioning from laboratory research to commercialization.

Coleman Murray

Coleman Murray is a Graduate Student Researcher working in the Microfluidic Biotechnology Laboratory under Professor Dino Di Carlo, at the University of California, Los Angeles. He received his BS in Mechanical Engineering from the University of California in Santa Barbara in 2010. His research focuses on high throughput filtration of bacterial and viral particles, electroactive microfluidics and magnetic cell manipulation.

Pietro Maoddi

Pietro Maoddi obtained a B.S. in Computer Engineering from Politecnico di Torino in 2009 and received his M.S. in Micro and Nano Technologies from Politecnico di Torino, Institut National Polytechnique de Grenoble and Ecole Polytechnique Fédérale de Lausanne in 2011. His interests focus on microfluidics, microsystems and microfabrication technologies in general.

Dino Di Carlo

Dino Di Carlo is an Assistant Professor in the department of Bioengineering at the University of California, Los Angeles where he directs the Microfluidic Biotechnology Laboratory. He received his B.S. in Bioengineering from the University of California, Berkeley in 2002 and received a Ph.D. in Bioengineering from the University of California, Berkeley and San Francisco in 2006. He then conducted postdoctoral studies from 2006–2008 at the Center for Engineering in Medicine at Harvard Medical School and Massachusetts General Hospital. His research aims to exploit the unique physics, microenvironment control, and the potential for automation associated with miniaturized systems for applications in basic biology, medical diagnostics, and cellular engineering.

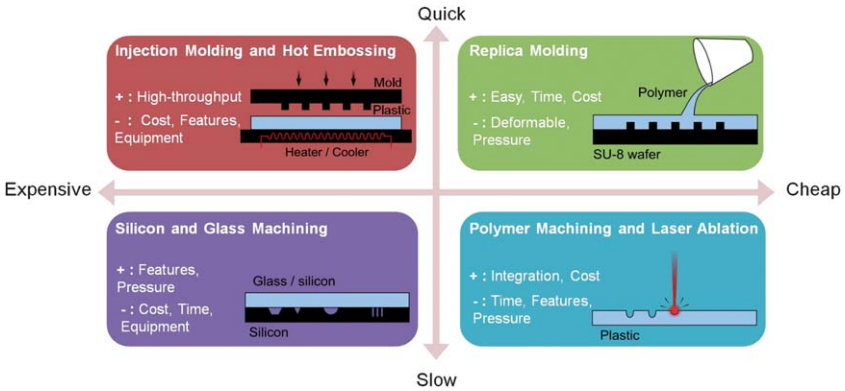

Fig. 1 Overview of microfluidic fabrication processes that can be used for prototyping.

demonstrated an improvement in the complete fabrication process, for a similar cost and time expenditure as PDMS,[9] by using inexpensive solid epoxy molds and optimization of thermal bonding. It remains to be seen whether these approaches will be more widely adopted by the microfluidics community.

(ii) Polymer ablation. Material from a polymer block can also be removed to form microstructures using direct write processes such as conventional mechanical drilling[14,15] and sawing, laser machining,[16] powder blasting, and dry film laminating.[22] In particular, *laser ablation* is also an advantageous alternative for prototyping, being cost-accessible and enabling complex 3D-multilayer structures.[12,23] For this method, a high-powered pulsed laser is used to remove material from a sheet of thermoplastic, like PMMA, PC, PVC and others, either through a mask or directly on the substrate.[13] The primary disadvantage of all these direct methods is their limited throughput, due to the inherent serial nature. These techniques also generate surface roughness on microchannels, reducing their overall optical efficiency, as well as debris that have to be removed from the device. Additionally, channels are usually larger than 50 μm and enclosed by laminated films with a weak bonding, which cannot withstand pressures above 30 PSI. Recent work specifically focused on reducing the roughness of channel sidewalls,[17] for example with femtosecond laser processing on PMMA.[10]

(iii) Polymer casting. Finally, *polymer casting* (also known as *replica molding* or soft lithography) is widely used for prototyping due to its precise replication, but without the need of expensive equipment, or advanced skills in microfabrication.[24] Specifically, polydimethylsiloxane (PDMS) has become a successful polymeric substrate material for rapid prototyping due to its low cost, simple fabrication, optical transparency, gas permeability, chemical inertness, adhesion to multiple substrates, non-toxicity, and ability to form multi level fluidic devices.[25,26]

PDMS drawbacks and alternatives

Despite the convenience of PDMS for rapid prototyping and its broad use in academic laboratories, PDMS has severe drawbacks which strongly limit the range of microfluidic applications. (i) PDMS has poor chemical compatibility with many organic solvents as it tends to swell upon contact, making it mainly suitable for aqueous applications. (ii) Modification of PDMS surfaces is unstable over time. (iii) PDMS adsorbs small molecules into its matrix, (iv) PDMS deformation under pressure is used for pneumatic valves and helps in mold replication, but can become a significant issue for high pressure operation as it leads to a large alteration of channel geometry. As an example, inertial focusing of cells requires a finite Reynolds number Re ($Re = \rho U_m D_H/\mu$, with ρ, U_m, μ being the density, maximum velocity, dynamic viscosity of the fluid, D_H the hydraulic diameter of the channel, defined as $D_H = 2WH/(W + H)$) and associated high flow rates, with pressure-induced channel deformation as a consequence. First, such deformation can affect fluidic resistance and increases the capacitive time constant for steady flow, making it difficult to accurately predict the flow rates in complex microfluidic networks. Second, precise knowledge of focusing positions for cytometry applications is critical in aligning the optical system. A shift in these positions, caused by channel deformation, may also distort the optical alignment. Third, channel walls fabricated in deformable material may also oscillate under pressure, creating lensing effects and variable focal length in the detection system. More generally, prototypes that function according to specifications in the laboratory environment may end up functioning abnormally when designs are transferred to rigid thermoplastics used for commercialization.

To reduce channel deformation, Inglis proposed to sandwich the PDMS channel between two glass slides, so that channel walls are completely-constrained and deformation is reported to be three times lower than for standard PDMS chips.[27] Such Glass-PDMS-Glass assembly is efficient but restricted to some applications. In parallel, Chiu *et al.* among others have worked to identify polymers complementary to PDMS, with similar fabrication procedures being characteristic of rapid prototyping but with higher rigidity and better resistance to solvents.[28–36] Fiorini *et al.* firstly explored Thermoset Polyester (TPE) as a complementary substrate material to PDMS.[28–30] Then, Polyurethane Methacrylate (PUMA) was proposed by Kuo *et al.* as a promising material especially for microdevices in clinical situations.[31–33] Commercial optical adhesives, such as Norland Adhesive 81 (NOA81), have been used later by Bartolo and others and propose similar advantages.[34–36] TPE, PUMA and NOA differ from PDMS in that the substrates are semi-cured first using UV light, removed from the master, and then allowed to completely cure against a cover to obtain the final bonded

channel. These non-elastomeric polymers are hard materials once cured.

This review systematically assesses these different polymer alternatives to PDMS for replica molding-based rapid prototyping, especially in view of high pressure injections with the specific example of inertial flow conditions. Often individual reports on alternative materials do not compare performance to other competing material replacements to PDMS. In this review we directly address this issue and compare these materials head-to-head in evaluating a variety of properties including: ease of fabrication, deformation under flow, capacitive flow stabilization time, channel bond strength, inertial focusing performance, biocompatibility, optical properties, and solvent compatibility. We emphasize here that these polymer alternatives, TPE, PUMA and NOA, have some considerable strengths for rapid prototyping when bond strength, predictable operation at high pressure, or transitioning to commercialization are considered important for the application, and hope this work provides a useful guide for use by the microfluidic community.

2. Microfluidic devices and ease of fabrication

Ease-of-use

A microfluidic prototyping material for a research laboratory environment should be easy to use. This includes having a short time to produce a chip, low technical difficulty, high repeatability, and high success rate. The success of PDMS as a prototyping material in the microfluidics community is due to it satisfying these criteria. Here we discuss these parameters for a range of prototyping materials beyond PDMS.

The time required for PDMS device production as indicated in Fig. 2 is roughly 3 h (1 h + 2 h of curing) once the silicon master is fabricated. Bonding for sealing of channels can be established between PDMS and PDMS, or other materials like glass or silicon. However, for many labs, PDMS bonding has variable success, depending on humidity and temperature, plasma equipment and power, ratio of crosslinking agent/polymer, and also last but not least, operator skill.[26] For example, for 10 PDMS chips, our success rate for chip sealing varies from 50 to 100% depending on the operator.

Fabrication using TPE, as described in Fig. 2, is also easy and quick (1 h) once the mold is generated, but a final curing step at room temperature requires 1 day. Contrary to PDMS, sealing of TPE to glass slides is highly reproducible, with high yield independent on the operator skill or environmental conditions.[28] As an indication, our success rate for chip fabrication and sealing was 90%. On 10 TPE chips, we obtained 9 homogenous and strong bonds, the failed bond being due to operator error and presence of air bubbles in the TPE mix. Moreover, TPE chips were also successfully sealed to other substrates like dielectric and metallic mirrors while PDMS does not form a permanent bond to these substrates. A drawback of TPE fabrication is the necessity of precisely weighing and mixing several components under a fume hood, due to the noxious fumes from the resin.

On the contrary, PUMA does not require handling under special ventilation. No mixing of components is required as the resin is directly poured on the mold and crosslinked under UV light. The fabrication is simple and a chip can be fabricated in a similar time as PDMS chips - 3 h (1 h + 2 h of cooling). The success rate for bonding is around 90% (for 10 chips and 3 devices/chip), with the failure mode being that the channels closer to the chip edges may not be well-sealed. Using a home-made suction system reduces bending of the polymer during demolding and improves homogeneity in bonding.[31]

Similarly to PUMA, prototyping with NOA does not require special manipulation precautions or mixing of components as the resin is directly poured into the mold. Bartolo *et al.*[34] present a method in which a thin NOA chip is sandwiched between two glass slides. The addition of this second glass slide, used to handle the thin NOA layer without bending, requires a drilling step, which complicates the fabrication process. A thicker NOA chip can be easily manipulated without this second glass slide. However, the fabrication of thicker devices is made challenging by the fast crosslinking time of the resin (only 1 or 2 s with our UV lamp) and thus requires fine tuning of the exposure dose to match with the thickness of the chip. Indeed, NOA in the center of a thick chip must be cured for correct demolding but a superficial uncured layer should still be present to allow subsequent sealing to a cover. We obtained 80% (for 10 chips and 3 devices/chip) as a success rate for chip fabrication and sealing, the main issue being the presence of residual uncured resin inside the channels leading to non uniform thickness.

Dimensions

The fidelity of the replication process for PDMS, TPE, PUMA and NOA was excellent for our devices and we confirmed the ability of these polymers to replicate a wide range of features for microfluidic systems. PDMS has already been cast against a suitable mold with sub-micron fidelity.[25,26,37] Fiorini *et al.* have demonstrated the ability of TPE to replicate a wide range of feature sizes and designs[29] whereas Kuo *et al.* reported a replication fidelity down to 2 μm.[32] Finally, Bartolo *et al.* validated the fabrication of NOA stickers with sub-micron size features.[34]

3. Channel deformation and robustness under high pressure

Mechanical properties of materials

To illustrate the deformability inside a microfluidic channel at high pressure and help in our material selection, tensile tests were carried out (Fig. 3). As a reference, Young's modulus is respectively 130 GPa for Silicon, 63 GPa for Pyrex Glass, 3 GPa for PMMA, and 2 GPa for PC[38] (Fig. 3.B).

TPE, NOA, PUMA, and PDMS cover a three order of magnitude range of stiffness from $\sim$ 1–1000 MPa (Fig. 3.A). PDMS can also have tunable stiffness by the addition of more or less cross-linking agent. As expected, the Young's modulus increases as the ratio of mixing is decreased (Fig. 3.C). In this way, the tensile modulus of PDMS can be varied from 0.8 to 2.5 MPa, for ratios between 1 : 20 and 1 : 5. A modulus of 2.5 MPa is reached for 1 : 10 ratio, which is the ratio generally recommended, and remains saturated around this value even if we double the amount of cross-linker from 1 : 10 to 1 : 5 (respectively 2.5 and 2.3 MPa). These results are consistant with the range of 0.5 to 4 MPa generally obtained and highly depending upon curing time and temperature.[24,26,39] For a ratio of 1 : 2, the

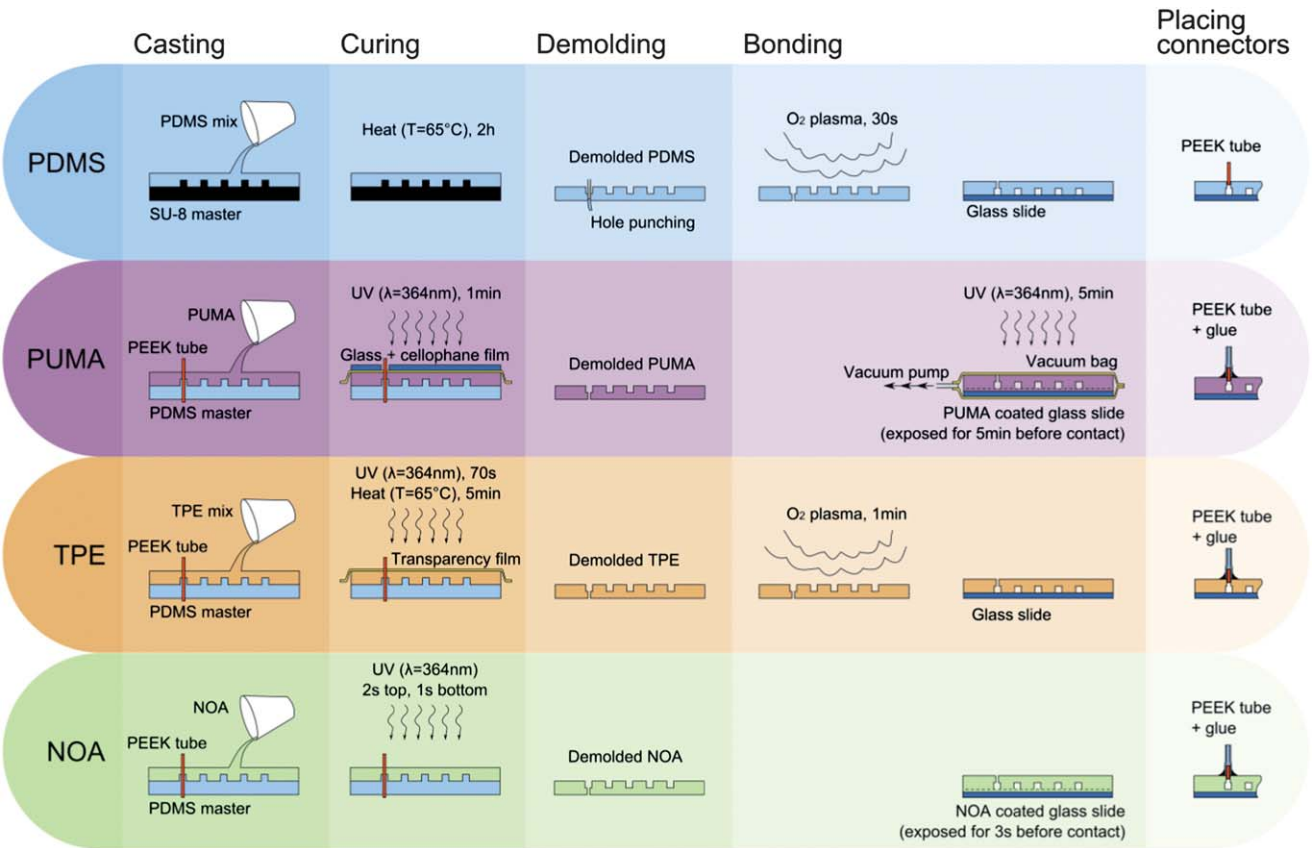

Fig. 2 Protocols for fabrication of PDMS, PUMA, TPE and NOA chips. Our primary test device was a straight and rectangular channel (5 cm long, 60 μm wide, 52 μm deep). A restriction (1000 μm long, 30 μm large) was added 4 cm downstream the inlet in order to validate the replication fidelity for more complex structures. **(i)** PDMS microfluidic devices were fabricated using standard replica molding processes,[26] with a cross linker to polymer ratio of 1 : 10, and maintaining 2 h as the curing time for repeatable mechanical measurements. As PUMA, NOA and TPE adhere to SU8 and make demolding impossible, a PDMS master mold with the same polarity as the silicon master was produced as indicated by Kuo *et al.*,[31] using octadecyltricholosilane (Sigma-Aldrich, 0.2% v/v in pure ethanol) to passivate the surface. **(ii)** The PUMA chips were prepared as previously described by Kuo *et al.*,[32] especially using 1 min of UV exposure for PUMA channels, 5 min for the PUMA-coated glass slide, and additional 5 mins to complete the bonding after the conformal sealing. **(iii)** TPE devices were fabricated following the protocol published by Fiorini *et al.*,[28–30] with UV exposure for 70 s in our conditions (λ = 364 nm, 400 W, Dymax Model 2000 Flood). **(iv)** NOA chips were made using a protocol adapted from Bartolo *et al.*[34] and Wägli *et al.*,[35] especially using 2 s of UV exposure for NOA channels, 3 s for the NOA-coated glass slide, and an additional 3 s to complete the bonding after the conformal sealing.

cured polymer is still sticky having some difficulties to crosslink (E = 1.1 MPa). These data confirm that changing the cross-linking ratio for PDMS is not a reliable solution towards more rigid polymer prototyping materials.

As discussed by Inglis,[27] recipes for harder PDMS have been recently developed as alternatives to classical Sylgard 184 PDMS. For example, the h-PDMS by IBM Zurich has been reported to be 4.5 times stiffer than standard PDMS[40,41] but Inglis reported difficulty in release of these polymers from the molds.[27] Here we tested another PDMS, also from Dow Corning with an expected higher stiffness (biomedical grade PDMS, Silastic 7-4860). Unfortunately, this Silastic PDMS is very viscous, which greatly complicates its processing, and above all still was measured to have a tensile elastic modulus similar to 1 : 10 PDMS (2.4 *versus* 2.5 MPa) (Fig. 3.A).

The other prototyping polymers investigated are much stiffer than PDMS. The Young's modulus measured for TPE is ~1.2 GPa, similar to thermoplastics like PC (2 GPa) and three orders of magnitude higher than 1 : 10 PDMS. This is important since design performance for TPE chips should be replicated when later transferring to mass producible thermoplastics, reducing the need to re-optimize designs late in the commercialization process. When cured as indicated in our process flow, NOA81 exhibits a tensile modulus of 325 MPa, which is lower than the 1 GPa reported by Bartolo *et al.*[34] but still two orders of magnitude higher than PDMS. As explained previously, such a difference is likely due to the reduced curing time that was required for successful device assembly and sealing. Finally, the tensile modulus measured for PUMA is 91 MPa, which is lower than TPE and NOA81. Notably, PUMA was observed to have different properties in its stress-strain curve than TPE and NOA81, with a short elastic behavior, for extension only from 0 to 2 mm, followed by a large plastic behavior, where PUMA pieces undergo irreversible extension up to 60 mm.

Deformation under flow

The low tensile modulus of PDMS offers several advantages for microfluidic applications as (i) it helps in demolding without

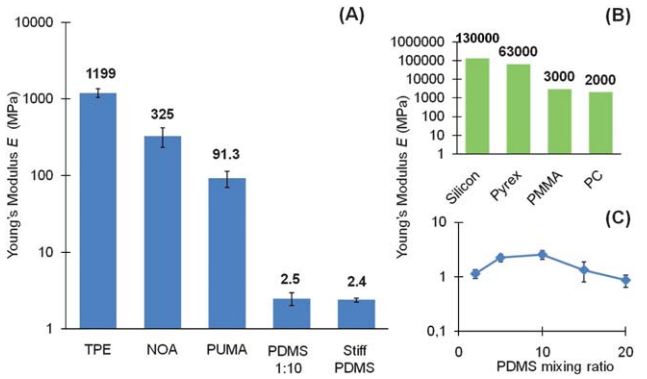

Fig. 3 Mechanical material properties for polymers used for chip fast-prototyping. Tensile elastic modulus (Young's Modulus, in MPa) was measured with an Instron instrument and is reported for a variety of materials. Raw data (Load as a function of extension) were converted into Strain and Stress and the slope for low strain was used to calculate the tensile elastic modulus (E). Identical rectangular specimens ($2 \times 26 \times 78$ mm) were measured on an Instron tensile tester (model 5564, 1 kN load, 10 mm/min). Three samples were characterized for each polymer. (A) Comparison of TPE, NOA, PUMA, 1 : 10 PDMS and stiff PDMS (Silastic). (B) The Young's moduli for Silicon, Pyrex Glass, PMMA and PC given by Laurell *et al.*[38] are shown for comparison. (C) Young's modulus as a function of mixing ratio between PDMS polymer base and crosslinking agent.

damage to features and (ii) can be used for specific microfluidic functions such as pressure-actuated valves demonstrated by Quake *et al.*[42] However, this unique property has also been shown to generate deformation of features and channels even under low pressure, potentially modifying device performance.

Only a few investigators have experimentally evaluated and discussed the extent of such deformation. Inglis directly used a bright-field microscope to assess the reversible deformation of a pillar-array at various pressures.[27] Gervais *et al.* used confocal microscopy for quantitative visualization of cross section expansion.[39] However, fluorescence microscopy consitutes a cheap and simple alternative for measuring channel deformation[43] which we employ in our comparisons (SI Figure 1†).

Microchannel deformation under continuous flow decreases substantially for more rigid prototyping polymers when compared to 1 : 10 PDMS (Fig. 4). **(1)** The largest deformations were obtained for PDMS-PDMS chips, where cross-sectional area expanded in both the X and Y directions (15.7% and 28.7%) at 300 μL/min. **(2)** For PDMS-Glass chips, the extent of the deformation in the depth is similar ($\Delta H = 20.5\%$ *versus* 28.7) however, the deformation in width is reduced by 56% ($\Delta W = 8.8\%$ *versus* 15.7%). The glass slide sealed to the channel is rigid ($E = 63$ GPa for Pyrex, Fig. 3.B), imposing a zero-displacement boundary condition along the PDMS-Glass interface.[27] Consequently, the channel roof can still move vertically but the bottom is constrained in all directions, reducing the lateral expansion of channel walls. **(3)** For all PDMS chips, we noticed a significant variation in deformation measurements (larger standard deviation error bars in Fig. 4) which may be due to slight differences in curing time and chip thickness, which are parameters that often vary for prototyping done in research labs. **(4)** As expected, assuming channels to deform according to their tensile modulus (Fig. 3), PUMA, NOA and TPE all exhibit less channel deformation than PDMS. PUMA channels linearly deform up to $\Delta W = 6.3\%$ and $\Delta H = 7.9\%$ at 400 μL/min. Deformation in channel depth for NOA is 66% lower than PDMS ($\Delta H = 7\%$)

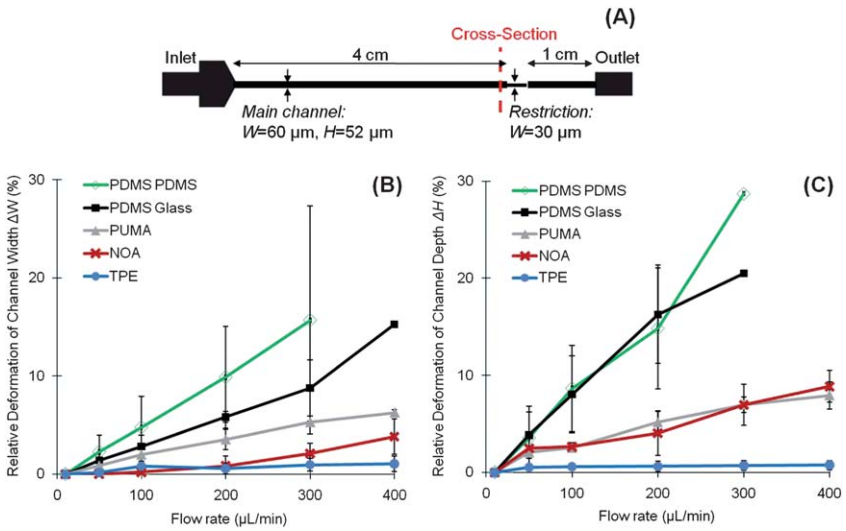

Fig. 4 Microchannel deformation as a function of flow rate for each polymer. (A) Schematic of the microchannel design. A straight channel ($W_C = 60$ μm, $H = 52$ μm, $L = 5$ cm) is implemented with a restriction ($W = 30$ μm, $L = 1000$ μm) located 4 cm downstream the inlet. Deformations are measured just before the restriction. (B, C) Deformations of channel width (B) and depth (C) *versus* flow rate. Images of fluorescein injections were recorded using a Photometrics CoolSNAP HQ2 CCD camera, a Nikon Eclipse Ti microscope, and Nikon NIS-Elements AR 3.0 software. Based on these images, the intensity profile of a given channel cross-section was plotted as a quantitative representation of cross-section shape and extension for each flow rate[43] (details of this measurement are presented in SI Figure 1†). The intensity measured at 10 μL/min was taken as a baseline because it was assumed that the channel cross section was not deformed under such a low flow rate. Relative changes in depth (ΔH) and width (ΔW) were defined as the normalized expansions in the X and Y axis respectively, compared to the 10 μL/min baseline, yielding the following equations; $\Delta W = W_{H/2}(Q)/W_{H/2}$(10μL/min) and $\Delta H = H(Q)/H$(10μL/min). Three measurements are done for each material - PDMS on PDMS (◇), PDMS on Glass (■), PUMA (▲), NOA (x) and TPE (●) - and each flow rate, varying from 10 to 400 μL/min.

and up to 76% smaller in width ($\Delta W = 2.1\%$). For TPE channels, measured expansions are almost zero (ΔW and ΔH less than 1%) even at 400 μL/min, with a reproducibility shown to be high. These results confirm TPE as the most rigid material and a good analogue to thermoplastics or glass, with lateral and longitudinal deformations considered negligible compared to PDMS channels.

Thus, even at low flow rates, the deformation of PDMS channels is significant in both X and Y directions, leading to channel cross-sections higher and wider than expected. Such channel expansion can greatly alter the flow in these channels or flow splitting in networks of channels. PUMA, NOA and especially TPE chips exhibit less deformation than PDMS which could bring some differences in flow and dynamic behavior as well as more predictable fluidic resistance values.

Dynamic behavior and pressure drop

An important demonstration of the effects of channel deformation on flow behavior is seen in observing the relationship between the flow rate and the total pressure drop. For steady state Stokes flow in rigid channels the pressure drop across the channel (ΔP) is known to be linearly related to the flow rate (Q) with the constant of proportionality being the fluidic resistance (R_{Hydr}). This leads to predictable analyses of microfluidic networks. Nonlinear relationships between pressure and flow rate lead to a loss of ability to engineer these networks effectively. Fig. 5.A illustrates the ΔP *vs.* Q relationship obtained for our tested devices.

(i) For all flow rates, the pressure measured in more deformable channels is less than the pressure in rigid TPE channels, indicating that the pressure required to drive the flow in deformable channels may be often over-estimated by calculations in nondeforming channels. For example, at 300 μL/min, the total pressure drop through the PDMS-PDMS, PDMS-Glass and PUMA channels was 67.6%, 51.7% and 31.8% less than through the rigid TPE channels. (ii) Inversely, for a given pressure, the flow rates are much higher than predicted in more deformable channels. For example, the flow rate expected in our rigid channel under a pressure of 60 PSI is 140 μL/min while it is measured to be 262 μL/min in the deforming PDMS-Glass channel, corresponding to a 187% increase in flow rate. Such a large difference is significant and has to be taken into account for device design during prototyping. (iii) Further, to complicate predictions of these differences, the pressure drop measured for PDMS channels depends nonlinearly with the flow rate.[34] These three effects of PDMS channel deformation impose a severe constraint on their design and use.

These results can be further explained by the analogy of any microfluidic network with an equivalent RC electric circuit (SI Figure 1.E†), the Hagen-Poiseuille law for a rigid channel ($\Delta P = R_{Hydr} \cdot Q$) being analogous to Ohm's law ($\Delta V = R_{Elec} \cdot I$), and the hydraulic compliance C_{Hydr} analogous to electric capacitance C_{Elec}.[44] (i) The high rigidity of TPE prevents channel distortion; compliance is negligible and the fluidic resistance is independent of pressure. Thus the line $\Delta P = RQ$ is close to the experimental pressure measured for the TPE device (●), with R being the fluidic resistance calculated using the initial channel dimensions (Fig. 5.A). (ii) Because of the high compliance of PDMS, the pressure distribution under an imposed flow rate deforms the channel shape ($R = f(P)$) considerably. Such deformation also varies down the channel length, because of the pressure gradient, and will modify the fluid velocity and the pressure distribution in return. Thus, the coupling between fluid flow and PDMS channel geometry is complex,[44] and makes it challenging to develop a simple and universal model.[39,43] To obtain a rough fit of pressure drops expected for PDMS channels, one can consider the model proposed by Gervais *et al.*[39] The channel walls are modelled as a semi-infinite medium and only the top wall is assumed to exhibit significant displacement, resulting in a steady state flow rate proportional to pressure to the fourth power (eqn (1)) and introducing nonlinearity into the pressure flow relationship.

$$Q = \frac{H_0^4 E}{48\mu\alpha(L-z)}\left(\left[1 + \frac{\alpha W}{EH_0}(P(z) - P(L))\right]^4 - 1\right) \quad \text{(Equation 1)}$$

In Fig. 5.A, we plotted this fit calculated for the tested microchannel (bottom fit with the main channel width, top fit with the restriction width) using the empirical value of $\alpha = 0.48$.[43] These fits agree with experimental results in general shape and magnitude, with differences in pressure drops being mainly due to a lower aspect ratio channel geometry ($W \approx H$) and an additional non-negligible pressure drop accross the outlet tubing.

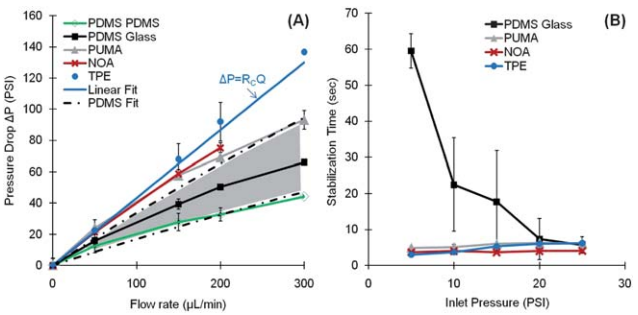

Fig. 5 Elasticity differences affect the pressure *vs.* flow characteristics and settling time. (A) The pressure drop measured at the inlet is plotted *versus* flow rate for PDMS on PDMS (◇), PDMS on Glass (■), PUMA (▲), NOA (x) and TPE (●) chips. Steady state pressure measurements were recorded using a pressure transducer (Honeywell ASCX150AN) placed in parallel with the chip inlet. The pressure signal was recorded by a Labview® virtual instrument at a sampling rate of 100 Hz. Pressure measured for TPE chips is close to linear theory (solid blue lines) for pressure drop through a rigid channel, where pressure is linearly proportional to flow rate and fluidic resistance calculated based on initial channel dimensions ($H = 52$ μm, $W_C = 60$ μm, $L_C = 5$ cm, $W_R = 30$ μm, $L_R = 1000$ μm). Pressure measured for deformable PDMS-Glass chips is compared to a theoretical model (dotted black lines)[39,43] setting a 3 mm top wall thickness (eqn (1)) and $E = 2.5$ MPa. (B) Stabilization or settling time as a function of inlet pressure, for PDMS on Glass (■), PUMA (▲), NOA (x) and TPE (●) channels. We measured the time required for 4.8 μm beads to stop their downstream motion after the pressure applied was changed from ΔP to 0 PSI. For high-precision measurements, sequences were recorded using a Phantom v7.3 highspeed camera (Vision Research Inc.) and Phantom Camera Control software. For both figures, three measurements were conducted for each material. Error bars represent standard deviation.

Dynamic behavior and stabilization time

In addition to steady state analysis, the tested materials varied in the transient behavior resulting from time-dependent flow changes. Flow stabilization time may be a practical limitation for some applications where a rapid dynamic response is essential, for example with stop-flow lithography[45] or with switching fluids for measuring fast kinetics.[46,47] Using a pressure control system - to reduce transients and long equilibration times - and rigid materials for all connecting parts and tubing, we evaluated transients solely due to material properties of the channels.

Given that the compliance of TPE, PUMA and NOA are negligible compared to PDMS due to their higher elastic moduli, the flow response time was expected and confirmed to be faster. Indeed, time delays in flow stabilization greatly increase for elastomeric microfluidic devices as elastomers capacitively store pressure applied to the system. As emphasized in Fig. 5.B, the stabilization time for PDMS varied from 60 s at 5 PSI to 7 s at 25 PSI, while the stabilization time for more rigid TPE, PUMA and NOA was consistently around 5–7 s for all tested pressures. Thus the relaxation time was up to 1200% higher in the PDMS than in TPE. These results are similar to those obtained by Bartolo *et al.*[34] and represent another concrete advantage of rigid polymers over PDMS.

Maximum pressure

High Reynolds number and associated high flow rates are required for many microfluidic phenomena, like inertial particle focusing and fast mixing to observe protein binding kinetics, among others. Additionally, nanofluidic systems have extremely high fluidic resistances. The challenge for such flows in microchannels and nanochannels is the significant pressure drop needed to drive the flow. For these reasons, the capability of a microfluidic device to withstand high pressure is a limiting factor for many systems and has to be quantitatively characterized towards the choice of the optimal substrate. Especially, as pressure drop has been previously shown to be much higher in rigid channels than in deformable ones for the same flow rate, the most rigid channels may be not the best-adapted to high pressures. Tests were conducted for each polymer to evaluate the pressure limit for the same microchannels, and maximum pressures obtained before failure are summarized in Table 1.

PDMS chips that we tested leak by delamination from the glass substrate at around 30–70 PSI. These data are consistent with the range of 30–50 PSI previously observed[25,26] and illustrate that PDMS may not be the best approach for high-pressure injections. PDMS connections, usually accomplished by compression fitting of tubing, are simple and reversible but leak at around 20 PSI. The addition of glues reinforces the connection however, delamination will still occur at slightly higher pressures. TPE chips are much more robust to high pressure. No leakage of the dye solution was detected outside of the channels up to 150 PSI, which corresponds to the upper limit of our pressure sensor, and illustrates the excellent quality of the TPE-Glass bond. These results are in good agreement with the value of 145 PSI (1 MPa) obtained previously.[28] PUMA sealing was measured to be at least 2 times stronger than PDMS, with maximum pressures superior to 100 PSI. These results are better than expected (40 PSI[32]) and confirm the advantage of PUMA over PDMS for high pressure flows. Finally, NOA chips exhibit maximum pressures around 70–80 PSI, which is still 2 times better than PDMS but almost 3 times lower than the 217 PSI previously reported.[34] It is likely that a further optimized NOA protocol for thick channels may provide better results for high-pressure injections.

Table 1 Measurements of maximum pressure (P_{max}) before failure for each polymer substrate and mechanism of failure. To evaluate P_{max} of each device, colored water was flowed through the devices with increasing flow rate while measuring the corresponding pressure until chip leakage was directly observed

Chip		P_{max} (PSI)	Failure Mode
PDMS on Glass	#1	51	Delamination
	#2	67	Delamination
	#3	36	Delamination
TPE	#1	150	Sensor limit
	#2	150	Sensor limit
	#3	150	Sensor limit
PUMA	#1	120	Connection leakage
	#2	110	Connection leakage
	#3	105	Delamination
NOA	#1	79	Delamination
	#2	74	Delamination
	#3	76	Delamination

4. Consequences for some flow patterns under high-pressure

These different consequences of material deformability have broad impacts in microfluidics, and should be carefully considered when choosing a prototyping material for a particular application. (i) The theoretical expectations of microfluidic behavior may be biased by incorrect predictions of geometries and flow/pressure profiles. (ii) Further, the deformation can alter the performance of devices. For example, such effects can be problematic for Inertial Focusing,[48,49] where the position of focused particle streams depends strongly on channel aspect ratio, or for Deterministic Lateral Displacement,[50] where operation strongly relies on precisely determined gap-distances between posts for accurate particle separation. Deformation affects pillars, which become narrower and increase the gap between each other as the pressure increases,[27] significantly changing this cut-off. (iii) Finally, if we consider fast prototyping as a step towards fabrication of commercial devices - like in rigid plastic cards - such differences in flow will require adjustments and optimization in the final device, increasing development cost. Thus, future experiments on any microfluidic phenomena and applications where a precise knowledge of the flow profile is required, should consider the effect of channel deformation and researchers should be aware of alternative materials that can resolve these effects.

In the following section, we mainly discuss two consequences of deformation under high pressure and consider how they affect two microfluidic phenomena. (*i*) *Cross-section deformation.* We especially consider how this deformation of the channel cross-section may alter the accuracy of particle manipulation by inertial focusing at high pressures.[51] (*ii*) *Acceleration along the channel.* Pressure drop has been reported to decrease nonlinearly along the length of a deformable channel due to the deformed

channel shape. A nonlinear pressure drop is accompanied by acceleration of the flow which may be a potential source of error for various calculations, for example on shear-stress.[39] We especially consider how this acceleration may affect vortex structures in successive expansion/contraction channels.

Cross-section deformation and consequence for inertial focusing

Recently, Di Carlo and others have shown that inertial focusing can separate microparticles and cells in microchannels.[49,52,53] Briefly, two inertial forces are involved: (i) a shear gradient lift force and (ii) a wall effect lift force,[48] inducing particle migration across streamlines when the particle Reynolds number Rp is of order 1 ($Rp = Re(a/H)^2$ with a the particle diameter). In rectangular or square channels, particles generally migrate to 2–4 distinct equilibrium positions which depend on the fold of symmetry of channel cross-section.[51]

Material deformability affects inertial focusing, presumably due to changes in channel cross-sectional shape and the overall channel symmetry. We injected 9.9 μm beads both in PDMS and TPE devices - TPE being the most rigid material - and compared particle distributions after 4 cm - ensuring complete particle ordering - and for different particle Reynolds numbers Rp (Fig. 6.A and B). 3D histograms are plotted for both materials to illustrate the variation of distribution as a function of Rp (Fig. 6. C and D) and more quantitative measurements are presented in Fig. 6.E. (i) As observed by Hur *et al.* in PDMS channels,[51] in both PDMS and TPE channels, initially randomly distributed particles began to migrate towards the channel centerline as Rp increased to 0.73 (50 μL/min). However, focusing in TPE was observed to be more accurate at earlier Rp (9 μm *vs.* 12 μm width of the focused stream in Fig. 6.E). (ii) As the flow rate increased ($Rp = 1.09$, 75 μL/min), particles started to occupy four focusing positions in PDMS channels, while only two positions are still distinguishable in TPE. Presumably, deformation in PDMS channels leads to a more four-fold symmetric cross-section with four equilibrium positions. (iii) At $Rp = 2.18$ (150 μL/min), beads in TPE channel also shift to lateral focusing positions. (iv) As Rp increased further ($Rp = 3.63$, 250 μL/min), particles in PDMS channels which are located in lateral positions, tend to move closer to the walls (Fig. 6.E). However, this displacement of lateral positions at higher flow rates is not observed in TPE

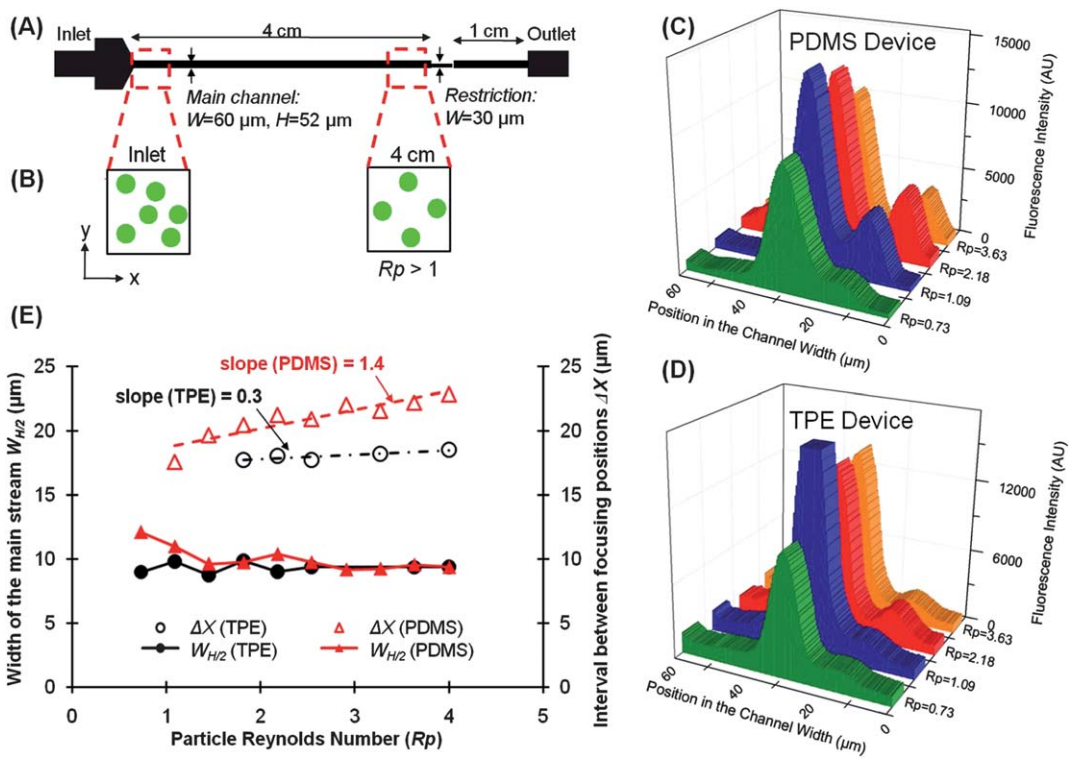

Fig. 6 Effect of material deformability on inertial focusing. (A) The microchannel design for inertial focusing is the same as for deformation studies, consisting of a straight channel ($W_C = 60$ μm, $H = 52$ μm, $L = 5$ cm) and a restriction ($W = 30$ μm, $L = 1000$ μm) located 4 cm downstream the inlet. Fluorescence images were captured in the middle y-plane, just before the restriction, to examine particle partitioning to dynamic equilibrium positions, assuming this distance is long enough for particles to be laterally focused.[48,51] (B) Schematic representation of the particle distribution in a rectangular channel. Experiments were conducted by flowing monodisperse 9.9 μm particles with flow rates varying from 25 to 275 μL/min. At the inlet of the channel, particles are randomly distributed. After 4 cm, particles flowing at $Rp > 1$ are inertially focused to four distinct equilibrium positions centered at the faces of the channels.[51] Distribution in a TPE channel should be affected by material rigidity. (C, D) 3D histogram illustrating particle alignment in the Y-direction and dependence on Rp, for PDMS and TPE. At $Rp = 0.73$, particles aligned into a single train for both materials. At $Rp = 1.09$, particles begin to align at four focusing positions in the Y-plane but only for PDMS. At $Rp = 2.18$, four positions are also distinguishable for TPE while at $Rp = 3.63$, lateral positions shift closer to the walls in PDMS channels. (E) Estimation of focusing accuracy for different Rp, and comparison between PDMS (red) and TPE (black). In particular, we determined the focusing width $W_{H/2}$ as the width at half of the maximum height extracted from a Gaussian fit. Particle focusing in TPE is measured to be more accurate at lower flow rates as the width of the main stream at $Rp = 0.73$ is smaller for TPE (●) than for PDMS (▲). The interval between focusing positions increases with Rp for PDMS (Δ) but remains constant for TPE (○).

channels, where the interval between focusing positions remains around 18 μm. Such a difference could be explained by the lateral expansion of the PDMS cross-section with increasing pressure, resulting in a lateral shift of focusing positions.

These results confirm that particle distribution, which is dependant on cross-section geometry, is also a function of material deformability. Thus, optimal fluidic conditions defined for focusing or separation in PDMS would have to be re-adapted in rigid devices to have a similar final performance.

Acceleration along the channel and consequences for vortices

The presence of laminar vortices (*i.e.* Moffatt's corner eddy flow) at sudden enlargements in microscale channels has been observed and studied in the fluid dynamic community.[54,55] Particle motion in these recirculations has been further investigated.[56–59] More recently, Hur, Mach *et al.*[60,61] demonstrated that these vortices can be utilized for size-based target cell separation with processing rates as high as 7.5 million of cells/s. In such applications, vortex size uniformity appears to be a crucial parameter to guarantee consistent performance. Here, we evaluate a similar design (*i.e.*, a straight channel with 8 reservoirs in series as represented in Fig. 7.A) to determine the effect of channel deformation on variation in vortex shape and size.

Vortex length increases with increasing channel deformation. In flow rates leading to vortex formation, the detachment of the boundary layer was observed at $R_C = 26.5$ for both PDMS and TPE channels. In these conditions PDMS deformation is low and has a negligible impact on the flow pattern we considered. For higher flow rates, deformation in width and depth are observed (SI Figure 2†). Especially, a significant deformation in PDMS channel height is observed in vortex reservoirs upstream, *i.e.* at higher pressure (from 23 to 8% for reservoir 1 to 8). Fig. 7.B demonstrates the flow pattern observed in the first reservoir while Fig. 7.C reports the vortex length for both TPE and PDMS as a function of reservoir number. Vortices in PDMS behave differently than in TPE, as indicated by differences in the slopes of linear fits. In rigid TPE channels, vortices have a similar shape and length whatever the reservoir location. However, for PDMS chips, vortex length decreases along the channel and towards the outlet, following a decrease in reservoir cross-section and an increase in velocity. In other words, successive reservoirs in the same PDMS chip exhibit different vortex structures, which are longer in a deformed reservoir than in a rigid one with the same initial dimensions. COMSOL simulations of flow patterns in vortices were conducted, assuming the deformed shape reported in SI Figure 1B.† The vortex length determined from these simulations is plotted in Fig. 7.C for each reservoir and confirms a decrease in vortex length for decreasingly deformed channels. Such a variation in vortex size is expected to result in non-uniform capturing of particles, with capture less efficient at the beginning of the channel. Researchers interested in controlling and utilizing these effects are strongly encouraged to consider rigid materials to increase consistency.

5. Other behaviors

Biocompatibility

Short term and long term cell viability was material-dependent after 2 and 24 h for HeLa cells incubated in TPE, PUMA and NOA chambers, and compared to 1 : 10 PDMS as a reference (Fig. 8). PDMS is well-suited to cell culture due to its permeability to oxygen and carbon dioxide which allow cells to respire normally.[25,62] PDMS, PUMA and NOA yielded similar cell viability after 2 h (between 82 and 90%). After 24 h, PUMA and

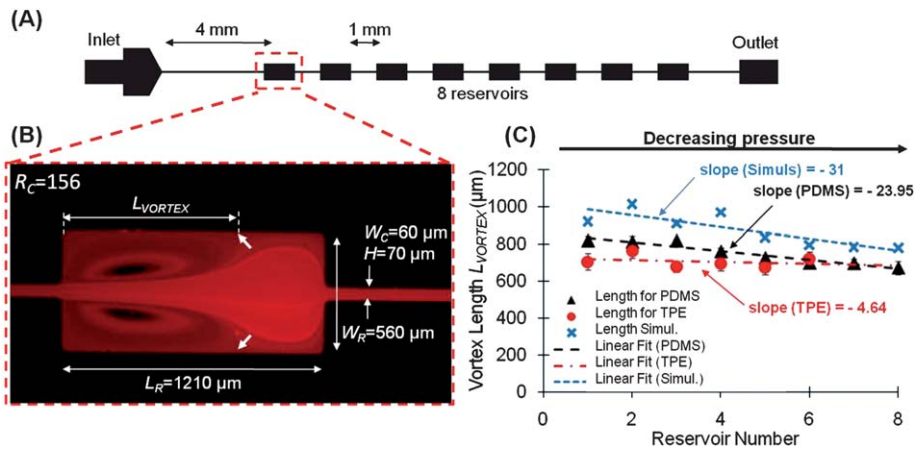

Fig. 7 Effect of material deformability on vortex flow field. (A) The microchannel design for vortex formation is shown. A straight channel ($W_C = 60$ μm, $H = 70$ μm, $L = 4$ mm) is implemented with 8 reservoirs ($W_R = 560$ μm, $L_R = 1210$ μm) located every 1 mm downstream. Filters located at the inlet prevented channel clogging by bead aggregates. (B) Vortices were visualized using 1 μm fluorescent particles. Flow rate is fixed at 400 μL/min, corresponding to a Reynolds number based on the channel width, $R_C = 156$. (C) Measured vortex length (L_{VORTEX}) *versus* the reservoir position along the microchannel, for four PDMS on Glass (▲) and two TPE (●) chips, at 400 μL/min. L_{VORTEX} corresponds to the length between the channel enlargement and the attachment point, and decreases with distance downstream (*i.e.* with decreasing pressure) for deformable PDMS channels, but is less dependent on position for rigid TPE channels. This general trend is also reported for vortex length determined by FEM simulations (**x**). We used COMSOL Multiphysics to numerically solve the Navier–Stokes Equations for incompressible fluid in the same channel geometry. From the solution, we were able to extract data such as the velocity field, streamlines, and L_{VORTEX} to compare with experiments.

NOA still maintained more than 85% viability, an improvement over PDMS which exhibited 70% viability (statistical significance = 0.018 and 0.029 in comparison with PUMA and NOA). These results agree with the known clinical biocompatibility of PUMA.[32,33,63] Similarly, NOA biocompatibility has already been verified with HeLa cells and neurons observed in microfluidic NOA stickers.[36,64] Contrastingly, TPE yielded a lower percentage of viable cells, around 80% even after 2 h of incubation. Previous uses of TPE for microfluidic chips have been mainly for electrophoresis and protein separation, such that its suitability for cell culture is largely unknown.[32] Nevertheless, this effect is not statistically significant with our sample size after static use (significance > 0.07), such that toxicity should not be a limiting problem for flow through applications.

Optical transparency

Optical transparency is important to consider for selecting a prototyping material. Especially, the detection of cells or small bioparticles may require direct observation or sensitive optical detection, such as fluorescence, when injected at high flow rates. Optical characterizations were previously reported for each material separately.[29,32,34,35,63] (i) All TPE, PUMA and NOA substrates have optical transmission similar to glass and PDMS in the visible range (400–800 nm) and can be directly placed on a microscope to examine cells or bioparticles. (ii) Due to the presence of UV photoinitiator for crosslinking, the transmittance of these materials quickly decreases below 400 nm, while glass and PDMS substrates transmit down to 300 nm and 240 nm respectively. Thus these UV-curing polymers are not particularly suitable for applications concerned with measuring UV absorbance of species within channels. (iii) Less autofluorescence is measured for PUMA than for TPE but still more than for PDMS. However, the autofluorescence level of the three substrates is shown to be similar to other thermoplastic materials and suitable for applications involving fluorescence detection. The autofluorescence level measured for 170 μm films made of NOA81 has been reported to be 4 times smaller than for the PDMS at 520 and 580 nm,[34] which also confirms NOA81 is well-suited to fluorescence detection-based applications.

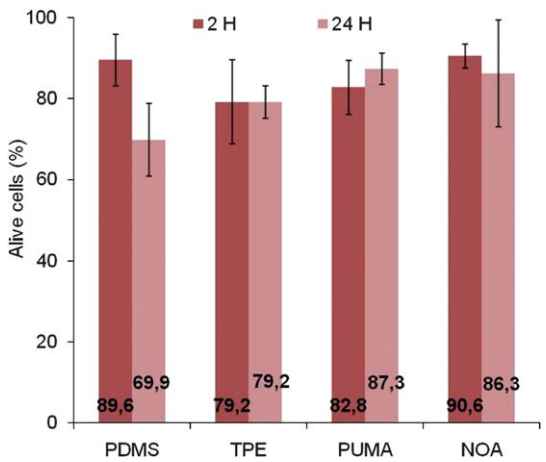

Fig. 8 Material biocompatibility measured with HeLa cells incubated in microchambers constructed of the polymers. HeLa cells cultured in RPMI medium 1640 with 10% FBS were trypsinized and resuspended in RPMI before use. Three square chambers, 1 × 1 cm, were designed for each polymer and each incubation time. All chambers were first rinsed with ethanol and incubated with 200 μL Fibronectin (50 μg/mL) at room temperature for 30 min. After removal of Fibronectin, 500 μL of HeLa cells were incubated at 37 °C in the wells and observed after 2 h and 24 h. Before observation, live cells were stained with 2 μM Calcein AM and dead cells with 4 μM EthD-1. The cells were then trypsinized and removed from suspension with DMEM. Green (live) and red fluorescent (dead) cells were counted using a hemacytometer.

Solvent compatibility

Solvent compatibility needs to be considered when choosing materials for specific analyses other than injection in water. Solvent resistant materials are needed since swelling can lead to premature device delamination, while solvent incompatibilities can lead to device cracking or reactant and assay contamination. Even for purposes beyond chemical synthesis on-chip, there is interest in using 70% ethanol and silicone oils in microfluidic devices. Ethanol is used as a sterilization agent for biological applications as well as a solvent for surface modifying chemical reactions, such as APTES surface coatings.[65] Additionally, there is a growing interest in droplet-based microfluidic systems in which silicone oils often are used. The solvent compatibility for PDMS, PUMA, NOA and TPE devices as separately reported in literature are compiled in a table (Fig. 9.A) while Fig. 9.B and C present our results obtained from injections of 70% ethanol and 1 cSt PDMS oil.

The well-known incompatibility of PDMS with many organic solvents strongly limits its range of applications to aqueous solutions.[60] For example, the PDMS devices we tested showed poor compatibility in 70% Ethanol, yielding a normalized failure flow rate of 68.6% compared to water injection, due to a strong and fast solvent-induced swelling of the device. Application of PDMS to droplet-based microfluidics is also challenging as the injection of oil solutions usually requires specific surfactants or a stable surface treatment. For example, PDMS devices are incompatible with 1 cSt PDMS oil, exhibiting immediate and significant swelling. TPE and PUMA have shown a greater resistance to swelling than PDMS for a wide range of solvents.[29,32] The TPE devices we tested exhibited an excellent compatibility with both 70% Ethanol and Silicone oil, with similar maximum flow rate (101 ± 2.37% and 100 ± 2.37%) and conservation of feature integrity. PUMA also exhibited a broad resistance to solvents, especially acetone, dyes, acids and bases. However, most organic solvents like ethanol at 100% purity are reported to cause PUMA swelling,[32] as confirmed by our tests in which PUMA exhibited total delamination upon contact with 70% ethanol. In contrast, the PUMA chips were compatible with 1 cSt PDMS oil showing neither reduction in normalized flow rate (100 ± 12.4%) nor swelling. NOA devices showed no solvent-induced swelling when injected with 70% ethanol or 1 cSt PDMS oil, which is consistent with previously reported results.[34,67,68] However, the failure flow rate in ethanol was found to be lower than for water, which has not been explained yet. The good compatibility of NOA with various solvents and oils explains the widespread use of thiolene devices for generation of solvent droplets as organic-phase micro-reactors.[34,36,67] These

(A)

Solvent	Swelling ratio			
	PDMS	TPE	PUMA	NOA
Water	1.00[L]	1.00[F]	1.0[K]	1.02[C]
Acetonitrile	1.01[L]	1.40[F]	1.1[K]	
Tetrahydrofuran	1.38[L]	1.50[F]	1.8[K]	1.49[C]
Methanol	1.02[L]	1.10[F]	1.4[K]	
Ethanol	1.04[L]	1.00[F]	1.4[K]	1.01[C]
2-Propanol		1.00[F]	1.2[K]	
Acetone	1.06[L]	1.40[F]	1.3[K]	1.31[C]
Ethyl Acetate	1.18[L]	1.30[F]		
Acetic Acid, 1M	1.00[L]	1.00[F]	1.0[K]	
Hydrochloric Acid, 1M	1.02[L]	1.00[F]	1.0[K]	
Ammonium Hydroxide, 1M	1.02[L]	1.00[F]	1.0[K]	
Sodium Hydroxide, 1M	1.01[L]	1.00[F]	1.0[K]	
Cyclohexane	1.33[L]	1.00[F]		
N-Heptane	1.34[L]	1.00[F]	1.1[K]	
Benzene	1.28[L]	1.10[F]		1.32[C]
Toluene	1.31[L]	1.00[F]		1.13[C]
Dimethyl Sulfoxide (DMSO)	1.00[L]		1.5[K]	
Formaldehyde			1.0[K]	
Fluorinert			1.0[K]	
Mineral Oil			1.0[K]	
Silicone oil			1.0[K]	
Perfluorodecalin	1.00[L]		1.0[K]	

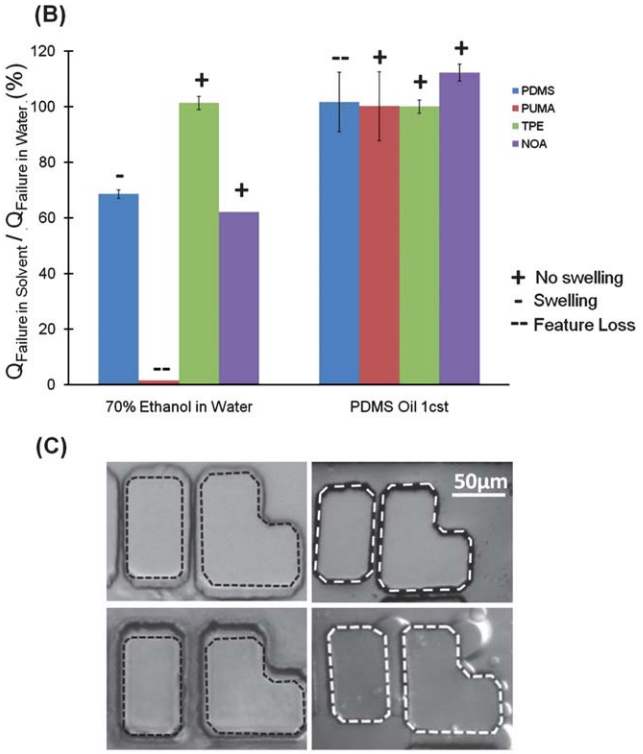

Fig. 9 Material solvent compatibility. (A) Table of swelling ratios for different solvents based on data reported by Lee *et al.*[L],[66] Fiorini *et al.*[F],[29] Kuo *et al.*[K],[32] and Cygan *et al.*[C].[67] These swelling ratios are obtained following the method previously proposed by Lee *et al.*,[66] which compares the lengths of solid pieces of each material before and after being immersed in a solvent for 24 h at 25 °C. (B) For each material, the maximum flow rate to chip failure for 70% Ethanol in water and 1 cSt PDMS oil (PDMS 200 fluid) were measured ($Q_{Failure\ in\ Solvent}$) and normalized to the maximum flow rate in water ($Q_{Failure\ in\ Water}$). In these experiments only, channels with larger geometry were used such that any solvent effects could be more easily observed. Additionally, each device was observed under a microscope during the tests to assess solvent induced device swelling. Feature integrity was evaluated with '+', '−' or ' - -' respectively indicating no swelling, swelling of features, or disappearance of features. (C) The effect of swelling on channel features was obtained by examining the features before and after solvent injection, where a dotted line represents the original geometry. The top and bottom left are PDMS channels injected with 1cSt PDMS oil and 70% ethanol in water respectively. The top and bottom right are TPE channels with 1 cSt PDMS oil and NOA channels with 70% ethanol in water.

experiments confirmed the good chemical resistance of TPE, PUMA and NOA to solvent solutions and their suitability as alternatives to PDMS for critical microfluidic applications where solvents are required.

6. Overall performance of replica molded polymer microfluidic devices

As summarized in Table 2, rapid prototyping in PDMS is advantageous because of its low cost, quick and straightforward fabrication, and its biocompatibility which allows its use for many applications. Nevertheless, its elastomeric nature and low elastic modulus result in many drawbacks. Indeed, even at low flow rates significant channel deformation occurs as the channel inlet pressure increases. This distortion introduces a non-linearity into the pressure flow relationship and the associated stabilization time can reach some minutes, even some hours for viscous fluids.[34] Further, the sealing to glass substrates fails at around 30–50 PSI, making PDMS devices inappropriate for high pressure injections.

Fabrication in TPE is more complex but still accessible, quick and cheap. TPE bonding was found to be highly reproducible and stronger than PDMS. The high rigidity of TPE, similar to glass, is also of great interest for high pressure injections as it prevents channels from being deformed. TPE compliance is negligible and fluidic resistance is not dependent on the pressure, thus resulting in a linear relationship between pressure drop and flow and a fast stabilization time. Its main limitation is its lower and relatively unknown biocompatibility for long-term cell culture.

The PUMA and NOA fabrication processes are simpler than for TPE and biocompatibility has already been validated for clinical devices for PUMA. The suitability of PUMA and NOA for high pressures lies between PDMS and TPE as the sealing strength is weaker than for TPE but still higher than PDMS, and channel deformation is still visible with PUMA when pressures increase.

All polymers tested (TPE, PUMA and NOA) (i) show good transmission in the visible light region but similarly block UV light, (ii) can be replicated over a wide range of feature sizes, and (iii) possess a solvent resistance better than PDMS. For these reasons, TPE, PUMA and NOA are promising alternatives to PDMS for rapid prototyping for high pressure or geometrically sensitive applications.

Table 2 Overall performance of PDMS, TPE, PUMA and NOA as materials for rapid prototyping of microfluidic devices and high pressure injections

		PDMS	TPE	PUMA	NOA
Material properties	Hardness	–	++	+	+
	Biocompatibility	+	–	++	++
	Optical Transparency	++	+	+	+
	Solvent Compatibility	–	+	+	+
Performance for Fast Prototyping and High Pressure Injections	Ease of Use	+	–	++	++
	Fabrication Time	1h + 2h	1h + 1day	1h + 2h	1h + 2h
	Cost	<$1/mL	~$4.5/mL	~$2.2/mL	<$1/mL
	Replication Fidelity	+	+	+	+
	Channel Deformation	–	++	+	+
	Stabilization time	–	++	++	++
	Maximum Pressure	–	++	+	+
	Inertial Focusing	–	++	+	+

7. Conclusion

Since the evaluated polymers all have advantages and disadvantages, the choice of the material will depend on the application. For applications coupling microfluidics with optical analysis, such as inertial focusing and flow cytometry, for which an accurate prediction of particle alignment is required, channel deformation and resulting pulsation of channels is the main issue to consider. Because of its higher rigidity, TPE is suggested as the material of choice for such applications. We also believe TPE is the best alternative to PDMS for particularly high pressures or for situations demanding fast flow-stabilization like in stop-flow lithography. For applications where biocompatibility is crucial, PUMA and NOA will be both perfectly suitable, with an advantage for PUMA which has already satisfied all clinical accreditations. In applications that involve chemicals or surface treatment, such as droplet microfluidics, TPE and NOA are particularly adapted thanks to their excellent compatibility with most oils and solvents.

Acknowledgements

We firstly thank Westbrook Weaver for his assistance with chemistry and clean room fabrication, Hamed Amini for his advice with Comsol simulations, Albert Mach for his help with our pressure set-up, and Dr Amy Chung for helpful discussions about the Instron equipment and tensile tests. We are really grateful to Dr Jason Kuo for his numerous advices about TPE and PUMA fabrication. We also thank Philip Wägli and Nicolas Champagne for NOA protocol, and John Oakey for the Silastic PDMS. This material is based upon work supported by grant number W81XWH1010519 from the Department of Defense Congressionally Directed Medical Research Program, and grant N66001-10-1-4072 from the Defense Advanced Research Projects Agency.

References

1 G. S. Fiorini and D. T. Chiu, Disposable microfluidic devices: fabrication, function, and application, *BioTechniques*, 2005, **38**, 429–446.
2 D. R. Reyes, D. Iossifidis, P. A. Auroux and A. Manz, Micro Total Analysis Systems. 1. Introduction, Theory, and Technology, *Anal. Chem.*, 2002, **74**, 2623–2636.
3 D. J. Beebe, G. A. Mensing and G. M. Walker, Physics and applications of microfluidics in biology, *Annu. Rev. Biomed. Eng.*, 2002, **4**, 261–286.
4 C. M. Klapperich, Microfluidic diagnostics: time for industry standards, *Expert Rev. Med. Devices*, 2009, **6**, 211–213.
5 S. D. Senturia, 2001, *Microsystem design*, Springer.
6 M. Napoli, P. Atzberger and S. Pennathur, Experimental study of the separation behavior of nanoparticles in micro and nano-channels, *Microfluid. Nanofluid.*, 2010, **10**, 69–80.
7 E. Sollier, H. Rostaing, P. Pouteau, Y. Fouillet and J. L. Achard, Passive microfluidic devices for plasma extraction from whole human blood, *Sens. Actuators, B*, 2009, **141**, 617–624.
8 R. M. Tiggelaar, F. Benito-Lopez, D. C. Hermesa, H. Rathgen, R. J. M. Egberink, F. G. Mugele, D. N. Reinhoudt, A. Van den Berg, W. Verboom and H. J. G. E. Gardeniers, Fabrication, mechanical testing and application of high-pressure glass microreactor chips, *Chem. Eng. J.*, 2007, **131**, 163–170.
9 E. W. K. Young, E. Berthier, D. J. Guckenberger, E. Sackmann, C. Lamers, I. Meyvantsson, A. Huttenlocher and D. J. Beebe, Rapid prototyping of arrayed microfluidic systems in polystyrene for cell-based assays, *Anal. Chem.*, 2011, **83**, 1408–1417.
10 R. Suriano, A. Kuznetsov, S. M. Eaton, R. Kiyan, G. Cerullo, R. Osellame, B. N. Chichkov, M. Levi and S. Turri, Femtosecond laser ablation of polymeric substrates for the fabrication of microfluidic channels, *Appl. Surf. Sci.*, 2011, **257**, 6243–6250.
11 H. Becker and U. Heim, Hot embossing as a method for the fabrication of polymer high aspect ratio structures, *Sens. Actuators, A*, 2000, **83**, 130–135.
12 G. Marchand, P. Broyer, V. Lanet, C. Delattre, F. Foucault, L. Menou, B. Calvas, D. Roller, F. Ginot, R. Campagnolo and F. Mallard, Opto-electronic DNA chip-based integrated card for clinical diagnostics, *Biomed. Microdevices*, 2007, **10**, 35–45.
13 C. G. Khan Malek, Laser processing for bio-microfluidics applications, Part I, *Anal. Bioanal. Chem.*, 2006, **385**, 1351–1361.
14 I. R. G. Ogilvie, V. J. Sieben, B. Cortese, M. C. Mowlem and H. Morgan, Chemically resistant microfluidic valves from Viton membranes bonded COC and PMMA, *Lab Chip*, 2011, **11**, 2455–2459.
15 C. R. Friedrich and M. J. Vasile, Development of the micromilling process for high-aspect-ratio microstructures, *J. Microelectromech. Syst.*, 1996, **5**, 33–8.
16 H. Klank, J. P. Kutter and O. Geschke, CO_2-laser micromachining and back-end processing for rapid production of PMMA-based microfluidic systems, *Lab Chip*, 2002, **2**, 242–246.
17 Y. Huang, S. Liu, W. Yang and C. Yu, Surface roughness analysis and improvement of PMMA-based microfluidic chip chambers by CO_2 laser cutting, *Appl. Surf. Sci.*, 2010, **256**, 1675–1678.
18 H. Becker and C. Gärtner, Polymer microfabrication technologies for microfluidic systems, *Anal. Bioanal. Chem.*, 2007, **390**, 89–111.
19 J. Giboz, T. Copponnex and P. Mele, Microinjection molding ofthermoplastic polymers: a review, *J. Micromech. Microeng.*, 2007, **17**, R96–R109.
20 M. Noerholm, H. Bruus, M. H. Jakobsen, P. Telleman and N. B. Ramsing, Polymer microfluidic chip for online monitoring of microarray hybridizations, *Lab Chip*, 2004, **4**, 28–37.
21 E. Roy, M. Geissler, J. C. Galas and T. Veres, Prototyping of microfluidic systems using a commercial thermoplastic elastomer, *Microfluid. Nanofluid.*, 2011, **11**, 235–244.

22 P. Vulto, N. Glade, L. Altomare, J. Bablet, L. Del Tin, G. Medoro, I. Chartier, N. Manaresi, M. Tartagni and R. Guerrieri, Microfluidic channel fabrication in dry film resist for production and prototyping of hybrid chips, *Lab Chip*, 2005, **5**, 158–162.
23 C. Lancaster, M. Kokoris, M. Nabavi, J. Clemmens, P. Maloney, J. Capadanno, J. Gerdes and C. F. Battrell, Rare cancer cell analyzer for whole blood applications: Microcytometer cell counting and sorting subcircuits, *Methods*, 2005, **37**, 120–127.
24 G. M. Whitesides, E. Ostuni, S. Takayama, X. Jiang and D. E. Ingber, Soft lithography in biology and biochemistry, *Annu. Rev. Biomed. Eng.*, 2001, **3**, 335–373.
25 J. C. Mac Donald, D. C. Duffy, J. R. Anderson, D. T. Chiu, O. J. A. Schueller and G. M. Whitesides, Fabrication of microfluidic systems in poly(dimethylsiloxane), *Electrophoresis*, 2000, **21**, 27–40.
26 J. C. Mac Donald and G. M. Whitesides, Poly(dimethylsiloxane) as a material for fabricating microfluidic devices, *Acc. Chem. Res.*, 2002, **35**(7), 491–499.
27 D. W. Inglis, A method for reducing pressure-induced deformation in silicone microfluidics, *Biomicrofluidics*, 2010, **4**, 026504.
28 G. S. Fiorini, M. Yim, G. D. M. Jeffries, P. G. Schiro, S. A. Mutch, R. M. Lorenz and D. T. Chiu, Fabrication improvements for thermoset polyester (TPE) microfluidic devices, *Lab Chip*, 2007, **7**, 923–926.
29 G. S. Fiorini, R. M. Lorenz, J. S. Kuo and D. T. Chiu, Rapid prototyping of thermoset polyester microfluidic devices, *Anal. Chem.*, 2004, **76**, 4697–4704.
30 G. S. Fiorini, G. D. M. Jeffries, D. S. W. Lim, C. L. Kuyper and D. T. Chiu, Fabrication of thermoset polyester microfluidic devices and embossing masters using rapid prototyped polydimethylsiloxane molds, *Lab Chip*, 2003, **3**, 158–163.
31 J. S. Kuo, Y. Zhao, L. Ng, G. S. Yen, R. M. Lorenz, D. S. W. Lim and D. T. Chiu, Microfabricating high-aspect-ratio structures in polyurethane-methacrylate (PUMA) disposable microfluidic devices, *Lab Chip*, 2009, **9**, 1951–1956.
32 J. S. Kuo, L. Ng, G. S. Yen, R. M. Lorenz, P. G. Schiro, J. S. Edgar, Y. Zhao, D. S. W. Lim, P. B. Allen, G. D. M. Jeffries and D. T. Chiu, A new USP Class VI-compliant substrate for manufacturing disposable microfluidic devices, *Lab Chip*, 2009, **9**, 870–876.
33 J. S. Kuo and D. T. Chiu, Disposable microfluidic substrates: Transitioning from the research laboratory into the clinic, *Lab Chip*, 2011, **11**, 2656–2665.
34 D. Bartolo, G. Degré, P. Nghe and V. Studer, Microfluidic stickers, *Lab Chip*, 2008, **8**, 274–279.
35 P. Wägli, B. Y. Guelat, A. Homsy & N. F. de Rooij, 2010, Microfluidic devices made of UV-curable glue (NOA81) for fluorescence detection based applications, *Proc. Micro Total Analysis Systems 2010*, Groningen, Netherlands, 1937–1939.
36 L.-H. Hung, R. Lin and A. P. Lee, Rapid microfabrication of solvent-resistant biocompatible microfluidic devices, *Lab Chip*, 2008, **8**, 983–987.
37 Y. Xia, J. J. Mc Clelland, R. Gupta, D. Qin, X. Zhao, L. Sohn, R. Celotta and G. M. Whitesides, Replica molding using polymeric materials: a practical step toward nanomanufacturing, *Adv. Mater.*, 1997, **9**, 147–49.
38 T. Laurell, F. Petersson and A. Nilsson, Chip integrated strategies for acoustic separation and manipulation of cells and particles, *Chem. Soc. Rev.*, 2007, **36**, 492–506.
39 T. Gervais, J. El-Ali, A. Günther and K. F. Jensen, Flow-induced deformation of shallow microfluidic channels, *Lab Chip*, 2006, **6**, 500–507.
40 T. W. Odom, J. C. Love, D. B. Wolfe, K. E. Paul and G. M. Whitesides, Improved pattern transfer in soft lithography using composite stamps, *Langmuir*, 2002, **18**, 5314–5320.
41 K. M. Choi and J. A. Rogers, A photocurable poly(dimethylsiloxane) chemistry designed for soft lithographic molding and printing in the nanometer regime, *J. Am. Chem. Soc.*, 2003, **125**, 4060–4061.
42 T. Thorsen, S. J. Maerkl and S. R. Quake, Microfluidic large-scale integration, *Science*, 2002, **298**(5593), 580–584.
43 B. S. Hardy, K. Uechi, J. Zhen and H. P. Kavehpour, The deformation of flexible PDMS microchannels under a pressure driven flow, *Lab Chip*, 2009, **9**, 935–938.
44 H. Bruus, 2008, *Theoretical microfluidics*, Oxford University Press.
45 D. Dendukuri, S. S. Gu, D. C. Pregibon, T. A. Hatton and P. S. Doyle, Stop-flow lithography in microfluidic device, *Lab Chip*, 2007, **7**, 818–828.
46 P. B. Allen, G. Milne, B. R. Doepker and D. T. Chiu, Pressure-driven laminar flow switching for rapod exchange of solution environment around surface adhered biological particles, *Lab Chip*, 2010, **10**, 727–733.
47 P. Sabounchi, C. Ionescu-Zanetti, R. Chen and M. Karandikar, Soft-state biomicrofluidic pulse generator for single cell analysis, *Appl. Phys. Lett.*, 2006, **88**, 183901.
48 D. Di Carlo, Inertial microfluidics, *Lab Chip*, 2009, **9**, 3038–3046.
49 D. Di Carlo, D. Irimia, R. G. Tompkins and M. Toner, Continuous inertial focusing, ordering, and separation of particles in microchannels, *Proc. Natl. Acad. Sci. U. S. A.*, 2007, **104**(48), 18892–18897.
50 J. A. Davis, D. W. Inglis, K. J. Morton, D. A. Lawrence, L. R. Huang, S. Y. Chou, J. C. Sturm and R. H. Austin, Deterministic hydrodynamics: Taking blood apart, *Proc. Natl. Acad. Sci. U. S. A.*, 2006, **103**(40), 14779–14784.
51 S. C. Hur, H. T. K. Tse and D. Di Carlo, Sheathless inertial cell ordering for extreme throughput flow cytometry, *Lab Chip*, 2010, **10**, 274–280.
52 S. C. Hur, N. K. Henderson-MacLennan, E. R. B. McCabe and D. Di Carlo, Deformability-based cell classification and enrichment using inertial microfluidics, *Lab Chip*, 2011, **11**, 912.
53 A. A. S. Bhagat, S. S. Kuntaegowdanahalli and I. Papautsky, Inertial microfluidics for continuous particle filtration and extraction, *Microfluid. Nanofluid.*, 2008, **7**, 217–226.
54 H. K. Moffatt, Viscous and resistive eddies near a sharp corner, *J. Fluid Mech.*, 2006, **18**(01), 1–18.
55 W. Cherdron, F. Durst and J. Whitelaw, Asymmetric flows and instabilities in symmetric ducts with sudden expansions, *J. Fluid Mech.*, 2006, **84**(01), 13–31.
56 E. Sollier, M. Cubizolles, Y. Fouillet and J. L. Achard, Fast and continuous plasma extraction from whole human blood based on expanding cell-free layer devices, *Biomed. Microdevices*, 2010, **12**(3), 485–497.
57 D. Lim, J. Shelby, J. Kuo and D. Chiu, Dynamic formation of ring-shaped patterns of colloidal particles in microfluidic systems, *Appl. Phys. Lett.*, 2003, **83**, 1145.
58 J. Park and H. Jung, Multiorifice Flow Fractionation: Continuous Size-Based Separation of Microspheres Using a Series of Contraction/Expansion Microchannels, *Anal. Chem.*, 2009, **81**(20), 8280–8288.
59 M. Khabiry, B. Chung, M. Hancock, H. Soundararajan, Y. Du, D. Cropek, W. Lee and A. Khademhosseini, Cell docking within double grooved substrates in a microfluidic device, *Small*, 2009, **5** (10), 1186–1194.
60 S. C. Hur, A. J. Mach and D. Di Carlo, High-throughput size-based rare cell enrichment using microscale vortices, *Biomicrofluidics*, 2011, **5**, 022206.
61 A. J. Mach, J. H. Kim, A. Arshi, S. C. Hur and D. Di Carlo, Automated cellular sample preparation using a Centrifuge-on-a-Chip, *Lab Chip*, 2011, **11**, 2827–2834.
62 M. C. Belanger and Y. Marois, Hemocompatibility, biocompatibility, inflammatory and in vivo studies of primary reference materials low-density polyethylene and polydimethylsiloxane: a review, *J. Biomed. Mater. Res.*, 2001, **58**(5), 467–477.
63 J. S. Kuo, Y. Zhao, P. G. Schiro, L. Ng, D. S. W. Lim, J. P. Shelby and D. T. Chiu, Deformability considerations in filtration of biological cells, *Lab Chip*, 2010, **10**, 837–842.
64 M. Morel, D. Bartolo, J. C. Galas, M. Dahan and V. Studer, Microfluidic stickers for cell- and tissue-based assays in microchannels, *Lab Chip*, 2009, **9**, 1011–1013.
65 W. M. Weaver, S. Dharmaraja, V. Milisavljevic and D. Di Carlo, The effects of shear stress on isolated receptor-ligand interactions of Staphylococcus epidermidis and human plasma fibrinogen using molecularly patterned microfluidics, *Lab Chip*, 2011, **11**, 883–889.
66 J. N. Lee, C. Park and G. M. Whitesides, Solvent compatibility of poly(dimethylsiloxane)-based microfluidic devices, *Anal. Chem.*, 2003, **75**, 6544–6554.
67 Z. T. Cygan, J. T. Cabral, K. L. Beers and E. J. Amis, Microfluidic platform for the generation of organic-phase microreactors, *Langmuir*, 2005, **21**, 3629–3634.
68 P. Wägli, A. Homsy and N. F. de Rooij, Norland optical adhesive (NOA81) microchannels with adjustable wetting behavior and high chemical resistance against a range of mid-infrared-transparent organic solvents, *Sens. Actuators, B*, 2011, **156**, 994–1001.